

X-ray photoelectron spectroscopy analysis and band offset determination of CeO₂ deposited on epitaxial (100), (110), and (111)Ge

Yan Zhu, Nikhil Jain, and Mantu K. Hudait^{a)}

Bradley Department of Electrical and Computer Engineering, Virginia Tech, Blacksburg, Virginia 24061

Deepam Maurya, Ronnie Varghese, and Shashank Priya

Center for Energy Harvesting Materials and Systems (CEHMS), Virginia Tech, Blacksburg, Virginia 24061

(Received 8 October 2013; accepted 26 December 2013; published 17 January 2014)

The oxidation states, interface, and band alignment properties of physical vapor deposited CeO₂ films on epitaxial (100), (110), and (111)Ge were investigated by x-ray photoelectron spectroscopy (XPS). The cross-sectional transmission electron microscopy demonstrated the polycrystalline nature of the CeO₂ film. XPS analysis showed multiple Ce3d and Ce4d oxidation states with a mixture of Ce³⁺ and Ce⁴⁺ components existing in CeO₂. Angular resolved XPS investigations indicate that the CeO₂ films mostly consist of Ce⁴⁺ oxidation states while the Ce³⁺ oxidation states are preferentially present near the surface. The CeO₂/(100)Ge, CeO₂/(110)Ge, and CeO₂/(111)Ge structures showed almost identical valence band offset (VBO) values of 1.6, 1.5, and 1.6 eV, respectively, using XPS measurements from Ce3d core level (CL) peaks. These (VBO) values were also supported by XPS measurements from shallow Ce4d CL binding energy peaks. The conduction band offset values between CeO₂/Ge were ~1.3 eV using the measured optical bandgap of CeO₂. The XPS spectral analysis of cerium oxidation states and the measured band offset parameters for carrier confinement would offer an important path for the future design of Ge-based metal-oxide semiconductor devices. © 2014 American Vacuum Society. [<http://dx.doi.org/10.1116/1.4862160>]

I. INTRODUCTION

Aggressive scaling of gate length and gate oxide thickness in Si complementary metal-oxide-semiconductor (CMOS) transistors have aggravated the problems of higher power consumption and higher gate leakage current.^{1–3} In parallel, results on high mobility channel materials together with high- κ gate dielectric have shown a potential pathway toward replacing the traditional Si based CMOS technology in nano-scale transistors for higher performance and low standby power logic applications.^{4–10} Recently, Ge has attracted significant attention due to its high intrinsic electron and hole mobilities.^{11–13} Among various high- κ gate dielectrics, cerium oxide (CeO₂) is an attractive candidate as a gate dielectric material on Ge as it provides high dielectric constant in the range of 23–52,^{7,8,10,13} high refractive index (2.2–2.8),¹⁴ high dielectric strength (~25 MV/cm),^{8,14} moderate bandgap (3.0–3.6 eV),^{7,8,13} and high thermal and chemical stability.^{7,14} In fact, the most important consideration for utilizing CeO₂ as gate dielectric on Ge is the valence band and conduction band offset values, which should be larger than 1 eV to block the carrier injection from the semiconductor to the insulator.^{9,15} In respect of these considerations, the integration of CeO₂ on high mobility Ge as well as understanding of the interfacial properties are vital for advancing the further development of alternate CMOS. Besides, the research on CeO₂/Ge structure will provide understanding of the interfacial chemical properties that play deterministic role in controlling the gate leakage current in a transistor. Although extensive studies have been conducted on the x-ray photoelectron spectroscopy (XPS) analysis of both CeO₂ and Ge,^{4–6,16–19} no band offset values

between CeO₂ and Ge have been reported due to the complexity of cerium (Ce) binding energy peaks, which presents challenge for analyzing both structural and electrical properties of CeO₂ on Ge. It has been demonstrated that the carrier mobility of Ge can be enhanced by utilizing Ge channel with different crystalline orientations:⁴ hole mobility is high in (110)Ge²⁰ and electron mobility is high in (111)Ge.²¹ The lack of band offset parameters and influence of Ge orientation necessitate the systematic XPS analysis and detailed band offset studies of CeO₂ grown on crystallographically oriented (100)Ge, (110)Ge, and (111)Ge layers.

In this study, detailed XPS analysis was conducted to determine the band offset of CeO₂ on (100), (110), and (111)Ge. The experimental results revealed that the valence band offset (VBO) between CeO₂ and Ge is almost identical for all three Ge orientations and the VBO value was ~1.6 eV. The extracted conduction band offset (CBO) was ~1.3 eV using the measured optical band gap of CeO₂ by spectroscopic ellipsometry. These experimentally measured band alignment parameters between the CeO₂ and the crystallographically oriented Ge provide important design parameters toward future CeO₂/Ge based MOS devices.

II. EXPERIMENT

Unintentionally doped (UID) Ge layers were grown by solid source molecular beam epitaxy (MBE) on (100)/6°, (110), and (111)A epi-ready GaAs substrates. The Ge MBE growth chamber is separated from the III-V growth chamber to reduce the intermixing between Ge and III-V materials. These two growth chambers are connected by ultrahigh vacuum transfer chamber. The detailed information on Ge growth process and the structural properties of Ge/GaAs heterostructure with different orientation can be found elsewhere.^{11,12}

^{a)}Electronic mail: mantu.hudait@vt.edu

CeO₂ thin films with thicknesses of ~20 and ~1.5 nm were deposited at room temperature using electron-beam physical vapor deposition (PVD) technique. The thicknesses were monitored using the quartz crystal monitor. A chamber base pressure of ~10⁻⁶ Torr was realized prior to the deposition of CeO₂ film. The ultrahigh pure oxygen gas was introduced at a flow rate of ~5 sccm as the process gas with a delay of about 30 s after starting the CeO₂ deposition in order to substitute the loss of oxygen which could have resulted from source heating by the electron-beam. Cross-sectional transmission electron microscopy (TEM) was used to characterize the interface between CeO₂ and crystallographically oriented Ge epilayers. TEM samples were prepared using conventional mechanical thinning procedure followed by Ar⁺ ion milling.

The chemical bonding properties of CeO₂ thin films and the band alignment of CeO₂ on (100), (110), and (111)Ge were investigated using the PHI Quantera SXM XPS system with a monochromated Al-K α (energy of 1486.7 eV) x-ray source. To better understand the bonding characteristics of the CeO₂ thin films, angular resolved XPS measurements were performed with different exit angles of 25°, 45° and 75°, respectively. The VBO values between CeO₂ and Ge with different Ge orientation were determined by measuring the binding energy from core levels (CLs) of Ce3d/Ge3d and valence band maxima (VBM) of CeO₂ and Ge, respectively. Shallow CL binding energy spectra from Ce4d were also collected to confirm the VBO values obtained from Ce3d peaks. The schematic diagram of the structures used in this study is shown in Fig. 1. As shown in Fig. 1, XPS spectra were collected from three samples of each Ge orientation: (1) 1.5 nm CeO₂/80 nm Ge was used to measure the CL binding energy of Ce and Ge at the interface; (2) 20 nm CeO₂/80 nm Ge was used to measure the CL binding energy of Ce and VBM of CeO₂; (3) 80 nm Ge without the top CeO₂ layer was used to measure the CL binding energy of Ge and VBM of Ge. Native oxide on Ge surface was removed by wet chemical etching using deionized water for 5 s before loading into the XPS chamber. Sample charging was occurred during XPS measurement and was a particular problem on the fully oxidized materials.²²⁻²⁴ Compensation

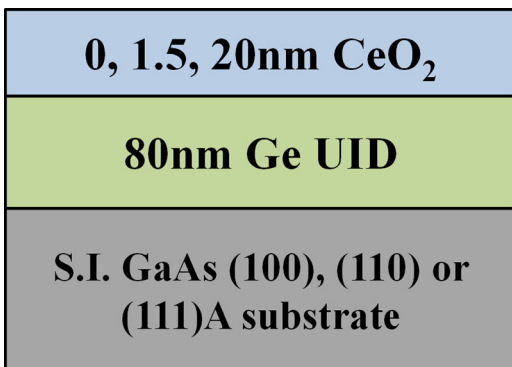


Fig. 1. (Color online) Schematic diagram of the CeO₂/Ge structures. 1.5 nm CeO₂/80 nm Ge was used to measure the CL binding energy of Ce and Ge at the interface, while 20 nm CeO₂/80 nm Ge and 80 nm Ge without the top CeO₂ layer were used to measure the binding energy of CeO₂ and Ge, respectively.

of the charging by an electron flood source was used in all measurements to minimize the binding energy shift. Besides, the measured CLs and VBM binding energy values were corrected by shifting C1s CL peak to 285.0 eV. All XPS spectra were recorded using pass energy of 26 eV and a step size of 0.025 eV. Curve fitting was done by the CasaXPS 2.3.14 using a Lorentzian convolution with a Shirley-type background. Different Ce core level peaks corresponding to various oxidation states and spin-orbit splitting levels were separated during curve fitting as reported in the literatures.^{18,19,25-28} For the Ce4d core level XPS spectra from 1.5 nm CeO₂/80 nm Ge samples, all Ce4d peaks were deconvoluted from the overlapped Ge3p_{1/2}, Ge3p_{3/2} core level and related oxidation states using reported Ge3p core level binding energy values.^{29,30}

After collecting the binding energy information from each sample surface, the VBO value can be determined by Kraut's method³¹

$$\Delta E_V = (E_{CL}^{Ge} - E_{VBM}^{Ge}) - (E_{CL}^{CeO_2} - E_{VBM}^{CeO_2}) + \Delta E_{CL}(i), \quad (1)$$

where E_{CL}^{Ge} and $E_{CL}^{CeO_2}$ are CL binding energies of Ge and CeO₂, respectively. For Ge, the Ge3d CL binding energy peak was used in the measurement; for CeO₂, the Ce3d CL peak was used for the determination of VBO and the shallow Ce4d CL binding energy was also used to confirm the VBO values obtained from Ce3d peaks. E_{VBM}^{Ge} and $E_{VBM}^{CeO_2}$ are the VBM of Ge and CeO₂, respectively. E_{VBM} of each material was determined by linearly fitting the leading edge of valence band spectra to the base line.³²⁻³⁴ $E_{CL}^{CeO_2} - E_{VBM}^{CeO_2}$ and $E_{CL}^{Ge} - E_{VBM}^{Ge}$ were measured from 20 nm CeO₂/80 nm Ge and 80 nm Ge without the top CeO₂, respectively. $\Delta E_{CL}(i) = E_{CL}^{CeO_2}(i) - E_{CL}^{Ge}(i)$ is the CL binding energy difference of Ce and Ge measured at the interface from 1.5 nm CeO₂/80 nm Ge of each structure. Once the VBO was obtained, the CBO can be estimated by³²⁻³⁴

$$\Delta E_C = E_G^{CeO_2} - \Delta E_V - E_G^{Ge}, \quad (2)$$

where $E_G^{CeO_2}$ and E_G^{Ge} are the band gap energies of CeO₂ and Ge, respectively. The band gap energy of CeO₂ film was determined by the Tauc's method³⁵ using variable angle spectroscopic ellipsometry employing a wavelength sweep from 300 to 800 nm at an increment of 5 nm.

III. RESULTS AND DISCUSSION

A. Material characterization

Figure 2 shows the cross-sectional TEM micrographs of CeO₂/(100)Ge/(100)GaAs heterostructure with different magnification. As shown in Fig. 2(a), there are no threading dislocations observed in Ge layer, as expected, due to the limited mismatch (~0.07%) between Ge and GaAs. The black spot in Fig. 2(a) is due to the artifact caused by sample preparation. A sharp heterointerface is displayed between Ge and (100)GaAs, indicating minimal interdiffusion which is

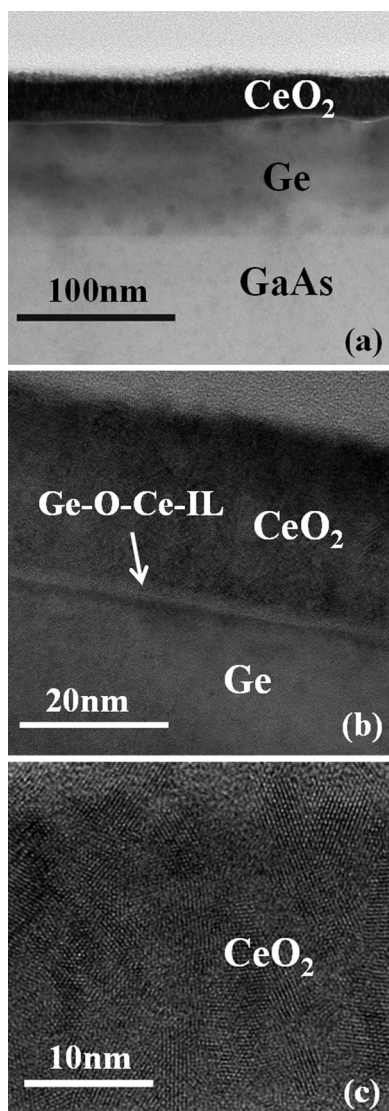


FIG. 2. Cross-sectional TEM micrographs of CeO₂/Ge/(100)GaAs heterostructure with different magnification. (a) A sharp heterointerface is displayed between Ge and (100)GaAs, indicating minimal atom interdiffusion; (b) The bright contrast at CeO₂/Ge interface shows the presence of an interfacial layer (~2 nm) consisting of the mixture of Ce-O-Ge formed spontaneously during oxide deposition; (c) The CeO₂ film deposited on (100)Ge is confirmed to be polycrystalline.

believed to be benefited from the separation of Ge and III-V MBE growth chambers. Figure 2(b) shows the interface between CeO₂ and (100)Ge with higher magnification revealing the presence of interfacial layer of ~2 nm formed spontaneously during the oxide deposition. Similar interfacial layer was also observed by other researchers at the CeO₂/Ge interface.³⁶ This interfacial layer between CeO₂ and Ge is noticeably different from the interfacial layer between Ge and other oxide materials, such as HfO₂ (Ref. 37) and Al₂O₃,³⁸ which exhibit sharp nonreacting heterointerfaces and also contain unstable components of GeO_x. Dimoulas *et al.*³⁶ reported that due to the catalytic properties of Ce, CeO₂ reacts strongly with Ge at the interface to produce an interfacial layer which contains a mixture of Ce-O-Ge oxide. Although other researchers reported that Ce

passivates the Ge surface and helps to stabilize Ge in one or two oxidation states,³⁶ this interfacial layer may increase the equivalent oxide thickness of the oxide stack and degrade the performance of MOS devices. Further investigation is needed to confirm these prior findings. The CeO₂ film deposited on (100)Ge was polycrystalline as evident from Fig. 2(c). The room temperature crystallization of CeO₂ was also reported on (100)Si by electron beam evaporation³⁹ and on (100)LaAlO₃ by pulsed laser deposition.⁴⁰ The room temperature crystallization of CeO₂ may attribute to the large kinetic energy of Ce obtained from high energy electron beam during PVD deposition which would enhance surface migration for epitaxy.⁴⁰

The optical band gap energy of CeO₂ on (100)Ge was measured using the Tauc's method by fitting the absorption spectra to the transition equation by extrapolating the linear portions of the curves to the base line as shown in Fig. 3. The transition equation can be expressed as

$$\alpha h\nu = E_D(h\nu - E_G)^{1/2}, \quad (3)$$

where α is the absorption coefficient, $h\nu$ is the photon energy, E_G is the optical band gap energy, and E_D is a constant which does not depend on the photon energy.⁴¹ The direct optical band gap of CeO₂ on (100)Ge was determined by plotting $(\alpha h\nu)^2$ versus $h\nu$ as shown in Fig. 3. Using this method, the optical band gap energies of CeO₂ were measured to be 3.6 eV. The measured optical band gap energies of CeO₂ are in close agreements with the results reported by other researchers.^{42–44}

B. X-ray photoelectron spectroscopy analysis of Ce oxidation states

Ce has two common oxidation states,^{17–19,25–28} Ce³⁺ and Ce⁴⁺, both of which were observed in Ce3d XPS spectra in this analysis. Figures 4(a)–4(c) show the Ce3d XPS spectra collected at an exit angle of 45° from 20 nm CeO₂ on (100), (110), and (111)Ge, respectively. As can be seen from Figs. 4(a)–4(c), there are 10 peak assignments within the Ce3d spectra on each Ge orientation. Different peak assignments

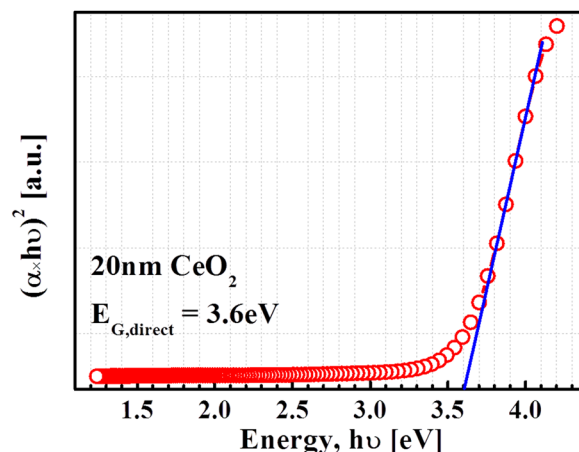


FIG. 3. (Color online) Direct optical band gap of CeO₂ on (100)Ge was determined to be 3.6 eV by plotting $(\alpha h\nu)^2$ vs $h\nu$.

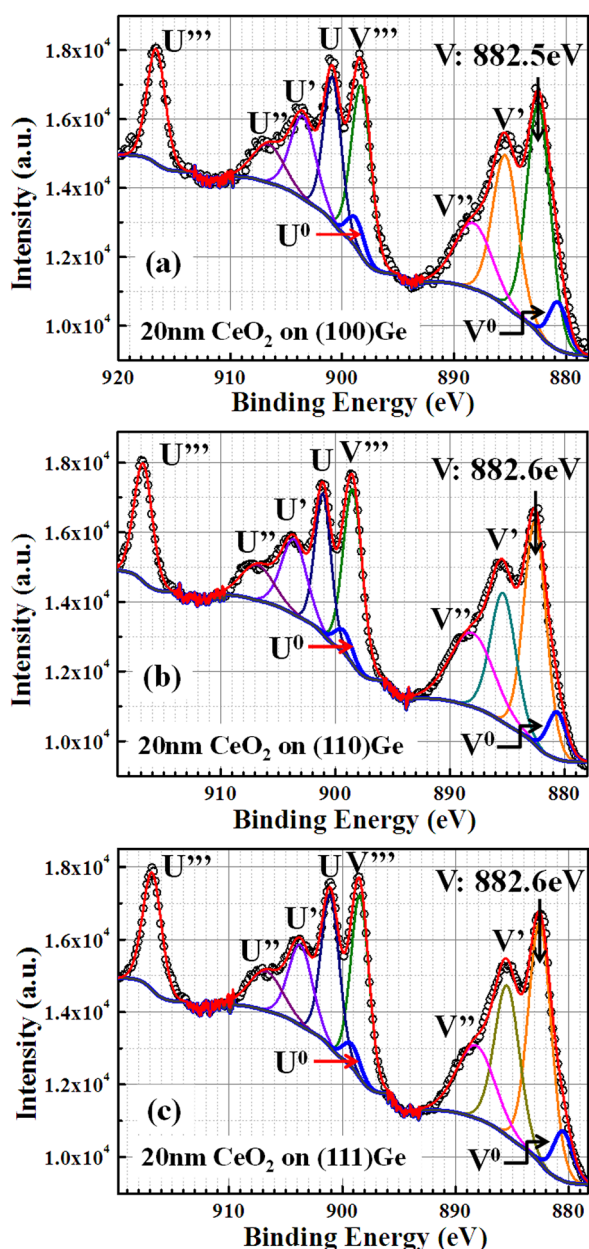


Fig. 4. (Color online) Ce 3d XPS spectra collected at an exit angle of 45° from 20 nm PVD deposited CeO₂ on (a) (100), (b) (110), and (c) (111)Ge, respectively. There are 10 peak assignments within the Ce 3d spectra on each Ge orientation. U and V refer to the 3d_{3/2} and 3d_{5/2} spin-orbit components, respectively. U, U'', U''', V, V'' and V''' refer to Ce⁴⁺ final states, while U⁰, U' and V⁰, V' refer to Ce³⁺ final states. The Ce⁴⁺3d_{5/2} binding energy peaks labeled as V were used to determine the band offset value between CeO₂ and Ge with each Ge orientation.

are labeled in the spectra following the convention established by Burroughs *et al.*,¹⁹ where U and V refer to the 3d_{3/2} and 3d_{5/2} spin-orbit components, respectively. Besides, U, U'', U''', V, V'' and V''' refer to Ce⁴⁺ final states, while U⁰, U' and V⁰, V' refer to Ce³⁺ final states.^{18,25–27} For Ce⁴⁺ peaks, the highest binding energy doublet U''''/V'''' at ~917 eV and ~898 eV are assigned to the final state of Ce⁴⁺3d⁹4f⁰ O2p⁶.¹⁸ The highest binding energy peak U'''' is the best distinguishing characteristic peak to differentiate Ce⁴⁺ and Ce³⁺ states, which is generally not observed for

pure Ce₂O₃.⁴⁵ Doublets U''/V'' at ~907 and ~889 eV were attributed to the hybridization state of Ce⁴⁺3d⁹4f¹ O2p⁵, and doublet U/V at ~901 and ~882 eV correspond to the state of Ce⁴⁺3d⁹4f² O2p⁴.¹⁸ For Ce³⁺ peaks, the doublet U'/V' at ~904 and ~886 eV corresponds to Ce³⁺3d⁹4f² O2p⁵ final states;³⁹ U⁰/V⁰ peaks at ~899 eV and ~881 eV relating to Ce³⁺3d⁹4f¹ O2p⁶ final states.^{25,26,28} All the measured Ce3d XPS peaks with different final oxidation states were summarized in Table I.

The total fraction of Ce₂O₃ in the PVD deposited CeO₂ on epitaxial Ge were estimated by taking the percentage of fitted Ce³⁺ spectral weight to the total weight of the spectra and calculated using the following equation:^{16,18,28}

$$\%Ce_2O_3 = \frac{Ce^{3+}}{Ce^{3+} + Ce^{4+}} = \frac{U^0 + V^0 + U' + V'}{U^0 + V^0 + \sum_{n'}(U^{n'} + V^{n'})}, \quad (4)$$

where n' is for all the final oxidation states. As there are no other Ce oxidation states detected in the CeO₂ films on epitaxial Ge except Ce⁴⁺ and Ce³⁺, the fraction of CeO₂ can be calculated by

$$\%CeO_2 = 1 - \%Ce_2O_3. \quad (5)$$

The fitted peak areas in the XPS spectra as shown in Figs. 4(a)–4(c) were used to estimate the contribution of Ce₂O₃ in the PVD deposited CeO₂ on (100), (110), and (111)Ge, respectively. The calculated Ce₂O₃ and CeO₂ fractions are also summarized in Table I. The percentage of Ce₂O₃ is 29.9%, 29.0%, and 28.3% within the PVD deposited CeO₂ on (100), (110), and (111)Ge, respectively, relating to the CeO₂ percentage of 70.1%, 71.0%, and 71.7% using an exit angle of 45°. As it has been reported that the Ce³⁺ oxidation state is preferentially present at the surface of the oxide film,¹³ angular resolved XPS measurements were performed in this study using a grazing exit angle of 25° and bulk-sensitive exit angle of 75° to identify the distribution. Detailed XPS analysis of the Ce3d spectra with different exit angles (spectra are not shown here) exhibited larger Ce³⁺ signal for the 25° grazing exit angle than for the 75° bulk-sensitive exit angle. The fitted peak positions and areas with different exit angles are also summarized in Table I. It can be seen from Table I that same final states, U⁰, U, U', U'', U''', U'''' and V⁰, V, V', V'', V''', V'''' were detected from the CeO₂ films with different exit angles. However, the percentage of Ce₂O₃ is 35.1%, 34.5%, and 34.7% within the CeO₂ films on (100), (110), and (111)Ge, respectively, using a grazing exit angle of 25° but reduced to 24.8%, 25.2%, and 24.3% using a bulk-sensitive exit angle of 75°, indicating that more fraction of Ce₂O₃ exists in the surface of the PVD deposited CeO₂ films. The reduction of Ce⁴⁺ oxidation states in CeO₂ films are also reported by other researchers, which is attributed to the result of the interaction with organics in the air before loading¹³ into the XPS chamber or due to x-ray exposure in vacuum during XPS measurements^{46,47} because of the catalytic properties of Ce. For convenience, we

TABLE I. Summary of peak position and relative area of Ce3d peaks with different final oxidation states. Three different exit angles were used to detect the percentage of Ce³⁺ final states within the PVD deposited 20 nm CeO₂ on (100), (110), and (111)Ge, respectively. The numbers in bold were picked up for band offset determination.

Peak assignment		Ce contribution		Exit angle																
				25°				45°				75°								
				Ge orientation																
				(100)	(110)	(111)	(100)	(110)	(111)	(100)	(110)	(111)	(100)	(110)	(111)	(100)	(110)	(111)		
		Peak (eV)	Relative area %	Peak (eV)	Relative area %	Peak (eV)	Relative area %	Peak (eV)	Relative area %	Peak (eV)	Relative area %	Peak (eV)	Relative area %	Peak (eV)	Relative area %	Peak (eV)	Relative area %	Peak (eV)	Relative area %	
	V ⁰	3+	880.7	4.3	880.8	4.5	881.0	4.7	880.9	3.7	880.8	3.9	881.0	3.9	881.1	2.9	881.0	2.8	880.9	2.8
	V	4+	882.4	23.6	882.6	22.5	882.5	22.7	882.5	22.4	882.6	21.1	882.6	22.2	882.5	22.9	882.6	24.2	882.5	23.6
	V'	3+	885.7	15.8	885.5	17.6	885.7	14.8	885.6	15.7	885.6	14.6	885.8	15.1	885.7	13.1	885.6	13.1	885.6	13.8
	V''	4+	888.7	7.6	888.9	7.3	888.7	7.2	888.6	9.9	888.5	12.9	888.9	11.1	888.6	11.8	889.0	10.2	888.9	10.9
Ce 3d _{5/2}	V'''	4+	898.5	14.7	898.4	13.5	898.6	14.1	898.5	13.7	898.5	14.2	898.8	13.2	898.6	15.8	898.6	15.6	898.5	15.5
	U ⁰	3+	899.2	2.7	899.0	2.6	899.1	2.8	899.1	2.0	899.3	1.7	899.2	1.6	899.1	1.4	898.9	1.2	899.0	1.1
	U	4+	900.9	7.4	900.8	10.9	900.9	10.1	901.0	10.5	901.3	9.7	901.2	11.1	901.2	9.2	901.2	10.4	901.1	9.8
	U'	3+	904.0	12.3	904.0	9.8	903.8	12.4	903.9	8.5	903.7	8.8	903.8	7.7	903.7	7.4	904.0	8.1	903.8	6.6
	U''	4+	907.2	3.3	907.4	2.8	907.4	3.2	907.3	4.9	907.2	4.9	907.3	5.3	906.9	7.4	907.1	5.9	906.7	6.9
Ce 3d _{3/2}	U'''	4+	916.9	8.3	916.7	8.5	916.8	8.0	916.8	8.7	916.8	8.2	916.9	8.8	916.8	8.2	916.9	8.5	916.8	9.0
Percentage of Ce ₂ O ₃			35.1		34.5		34.7		29.9		29.0		28.3		24.8		25.2		24.3	
Percentage of CeO ₂			64.9		65.5		65.3		70.1		71.0		71.7		75.2		74.8		75.7	

consistently refer to the layer as CeO₂ in this study, despite the possibly thin Ce³⁺ layer near the surface.

C. Band alignment of CeO₂/Ge structures using Ce3d core level states

XPS measurements were performed on all these structures with different CeO₂ thickness and different Ge orientations to determine the band offset values, as described above. Due to the strong binding energy signal and well defined peak shape, the Ce⁴⁺ final state Ce⁴⁺3d_{5/2}⁹4f²O2p⁴, labeled as peak V in Figs. 4(a)–4(c), were selected for the determination of band offset values. It should be noted that other Ce⁴⁺3d oxidation states were also used to verify the band offset values obtained from peak V and the VBO value difference is within ±0.1 eV, which is within the error range we labeled in this work. Figures 4(a) and 5(a) show the Ce3d CL and CeO₂ VB spectra from 20 nm CeO₂/80 nm (100)Ge. Figures 5(b) and 5(c) show Ge3d CL and Ce3d CL spectra measured from 1.5 nm CeO₂/80 nm (100)Ge at the interface, all of which are measured using an exit angle of 45°. As can be seen from the Ge 3d CL spectra shown in Fig. 5(b), both Ge-Ge and Ge-O bond states are detected. The Ge-O bond states may come from the interfacial layer at Ge/CeO₂

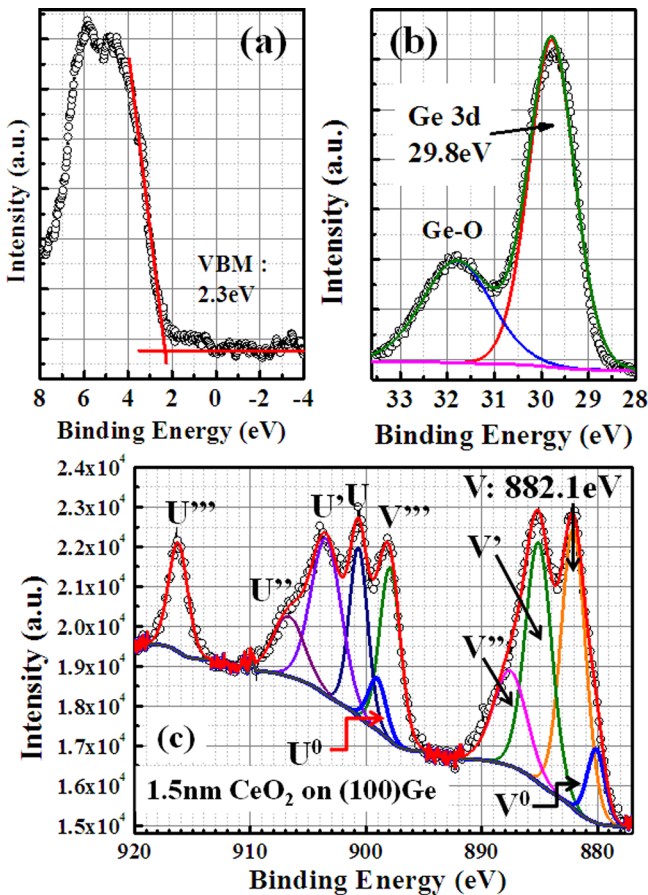


Fig. 5. (Color online) XPS spectra of (a) CeO₂ valence band from 20 nm CeO₂/80 nm (100)Ge; (b) Ge3d core level and (c) Ce3d core level spectra measured from 1.5 nm CeO₂/80 nm (100)Ge at the interface. Core level spectra curves were fitted using a Lorentzian convolution with a Shirley-type background. Valence band maxima were determined by linearly fitting the leading edge of the valence band spectra to the base line.

TABLE II. Summary of peak position and relative area of Ce3d peaks with different final oxidation states from 1.5 nm PVD deposited CeO₂ on (100), (110), and (111)Ge, respectively. An exit angle of 45° was used. The numbers in bold were considered for band offset determination.

Peak assignment	Cerium contribution	Ge orientation					
		(100)		(110)		(111)	
V ⁰	3+	880.8	3.8	880.7	3.9	880.8	3.9
V	4+	882.1	20.2	882.2	20.5	882.0	18.3
V'	3+	885.2	18.7	885.3	21.5	885.3	18.8
V''	4+	888.1	9.3	888.2	8.9	888.4	9.5
V'''	4+	898.1	10.6	898.2	8.0	898.2	11.4
U ⁰	3+	898.8	2.7	899.0	2.8	899.0	2.2
U	4+	900.6	9.2	901.0	11.5	900.7	8.4
U'	3+	903.4	13.9	903.5	11.9	903.3	14.1
U''	4+	906.9	5.5	906.8	6.5	906.8	7.3
U'''	4+	916.3	6.1	916.4	4.5	916.3	6.1
Percentage of Ce ₂ O ₃		39.1		40.1		39.0	
Percentage of CeO ₂		60.9		59.9		61.0	

interface as detected from the TEM analysis. Similar Ge-O peaks were also detected in early studies of the HfO₂ on Ge.^{4,5} The fitted peak positions and areas of Ce3d binding energy peaks from 1.5 nm CeO₂/80 nm (100)Ge structure are summarized in Table II. The Ge3d CL and Ge VBM binding energy from 80 nm (100)Ge without the top CeO₂ were pre-measured and can be found elsewhere.⁴⁻⁶ The CL to VBM binding energy difference for CeO₂ and (100)Ge are summarized in Table III. The results show that the value of ($E_{Ce^{4+}3d(V)}^{CeO_2} - E_{VBM}^{CeO_2}$) is about 880.2 eV. The premeasured value of ($E_{Ge^{3d}}^{Ge} - E_{VBM}^{Ge}$) is 29.5 eV, reported earlier in Ref. 6. The binding energy difference between the Ce⁴⁺3d_{5/2}(V) and the Ge3d states at the interface ($\Delta E_{CL}(i)$) was found to be 852.3 eV. Using these results, the VBO of (100)Ge with respect to CeO₂ is determined to be 1.6 ± 0.1 eV. The uncertain value of 0.1 eV is from the curve fitting process together

TABLE III. Summary of core level to valence band maxima binding energy difference (eV) for CeO₂ and Ge, and the binding energy difference between Ce⁴⁺3d_{5/2} (peak V) and Ge3d at the interface ($\Delta E_{CL}(i)$) from (100), (110), and (111)Ge, respectively, with an exit angle of 45°. The measured valence band offset (ΔE_V) is also listed in the table. The conduction band offset values are calculated using the band gap energy of Ge and the measured optical band gap energy of CeO₂.

Peak assignment	Ge orientation		
	(100)	(110)	(111)
$E_{Ce^{4+}3d(V)}^{CeO_2}$ (eV)	882.5	882.6	882.6
$E_{VBM}^{CeO_2}$ (eV)	2.3	2.4	2.5
$E_{Ge^{3d}}^{Ge} - E_{VBM}^{Ge}$ (eV) (Ref. 6)	29.5	29.4	29.6
$E_{Ce^{4+}3d(V)}^{CeO_2}(i)$ (eV)	882.1	882.2	882.0
$E_{Ge^{3d}(i)}^{Ge}$ (eV)	29.8	29.9	29.9
ΔE_V (eV)	1.6	1.5	1.6
ΔE_C (eV)	1.3	1.4	1.3

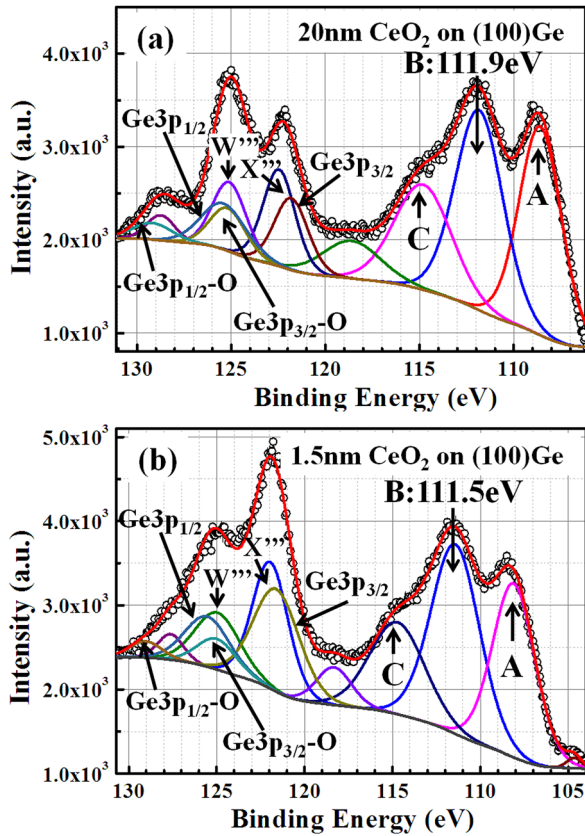


FIG. 8. (Color online) Ce4d core level XPS spectra measured from (a) 20 nm CeO₂/80 nm (100)Ge structure and (b) 1.5 nm CeO₂/80 nm (100)Ge structure. The Ce4d core level XPS spectra were deconvoluted to obtain all Ce4d peaks from the overlapped Ge3p_{1/2}, Ge3p_{3/2}, and related oxidation states. Core level spectra curves were fitted using a Lorentzian convolution with a Shirley-type background.

Mullins *et al.*²⁶ but were not identified. Besides, another peak at ~129 eV can be found from the Ce4d binding energy spectra in our study, which is absent in earlier studies. Further investigations are needed to identify the nature of this peak. Peak positions of Ce4d binding energy with different final oxidation states from 20 nm CeO₂/80 nm (100)Ge are summarized in Table IV. Ce4d and Ge3p as well as related oxidation state peak positions from 1.5 nm CeO₂/80 nm (100)Ge are summarized in Table V.

The Ce4d⁴⁺ final state labeled as peak B in Figs. 8(a) and 8(b) were used to determine the band offset value between CeO₂ and (100)Ge due to its well defined peak shape and strong intensity. The Ce4d⁴⁺ (peak B) CL to VBM binding energy difference for CeO₂ are summarized in Table VI. The $(E_{Ge3d}^{Ge} - E_{VBM}^{Ge})$ ⁶ and $[\Delta E_{CL}(i) = E_{Ce4d(B)}^{Ce}(i) - E_{Ge3d}^{Ge}(i)]$ values are also summarized in Table VI. Using these results, the VBO of (100)Ge with respect to CeO₂ was determined to be 1.6 ± 0.1 eV, which is in agreement with VBO value obtained using Ce3d CL peaks. Similar measurements were also performed on CeO₂/(110)Ge and CeO₂/(111)Ge structures. The Ce4d CL spectra from CeO₂/(110)Ge and CeO₂/(111)Ge with different CeO₂ thickness are shown in Figs. 9(a), 9(b), 10(a), and 10(b), respectively. Tables IV and V summarized the Ce4d CL peak positions from 20 nm

TABLE IV. Summary of peak position of Ce4d binding energy peaks with different final oxidation states from 20 nm PVD deposited CeO₂ on (100), (110), and (111)Ge, respectively. An exit angle of 45° was used. The Ce4d core level XPS spectra were deconvoluted to obtain all Ce4d peaks from the overlapped Ge3p_{1/2}, Ge3p_{3/2}, and related oxidation states. The numbers in bold were considered for band offset determination.

Peak assignment	Cerium contribution	Ge orientation		
		(100)	(110)	(111)
A	4+	108.7	108.7	108.8
B	4+	111.9	111.9	112.1
C	4+	115.1	114.8	115.5
Ge3p _{3/2}	—	121.7	121.6	121.8
X'''	4+	122.4	122.2	122.6
W'''	4+	125.7	125.4	125.8
Ge3p _{3/2} -O	—	125.8	125.5	125.9
Ge3p _{1/2}	—	125.9	125.6	126.0
Ge3p _{1/2} -O	—	129.3	129.5	129.6

CeO₂/80 nm Ge and 1.5 nm CeO₂/80 nm Ge with different Ge orientations, respectively. The measured values of $(E_{Ce4d(B)}^{CeO_2} - E_{VBM}^{CeO_2})$ and $(\Delta E_{CL}(i))$ from CeO₂/(110)Ge and CeO₂/(111)Ge are summarized in Table VI. The calculated VBO is 1.6 ± 0.1 eV for CeO₂/(110)Ge and 1.6 ± 0.1 eV for CeO₂/(111)Ge, both of which are in close agreement with the VBO values obtained from Ce3d CL peaks. The small difference in VBO value may be caused by the fitting of CL peaks and the VBM position. The CBO of all three structures were calculated from Eq. (2) and also summarized in Table VI.

Figure 11 shows the schematic band alignment diagram for the CeO₂/Ge structures based on the results presented above. The measured VBO and calculated CBO are also labeled in this figure. Figure 12 shows the histogram of ΔE_V and ΔE_C distribution of PVD deposited CeO₂ on (100), (110), and (111)Ge, respectively. It can be seen from this figure that although the band gap energy of CeO₂ is lower compared with other common used high- κ gate dielectric such as

TABLE V. Summary of peak position of Ce4d binding energy peaks with different final oxidation states from 1.5 nm PVD deposited CeO₂ on (100), (110), and (111)Ge, respectively. An exit angle of 45° was used. The Ce4d core level XPS spectra were deconvoluted to obtain all Ce4d peaks from the overlapped Ge3p_{1/2}, Ge3p_{3/2}, and related oxidation states. The numbers in bold were considered for band offset determination.

Peak assignment	Cerium contribution	Ge orientation		
		(100)	(110)	(111)
A	4+	108.2	108.3	108.1
B	4+	111.5	111.6	111.5
C	4+	114.8	114.6	114.9
Ge3p _{3/2}	—	121.6	121.6	121.5
X'''	4+	121.9	122.0	121.9
W'''	4+	125.0	125.1	125.0
Ge3p _{3/2} -O	—	125.1	125.0	124.8
Ge3p _{1/2}	—	125.6	125.5	125.4
Ge3p _{1/2} -O	—	129.1	129.0	128.8

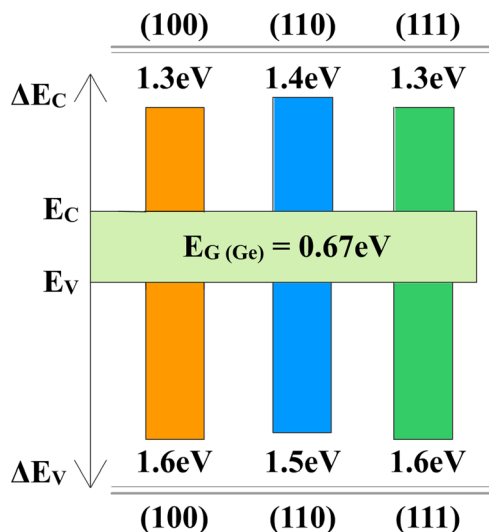


FIG. 12. (Color online) Histogram of band offset distribution obtained from CeO₂/Ge interface with different Ge orientations.

IV. CONCLUSION

CeO₂ oxide layers were deposited using physical vapor deposition on epitaxial (100), (110), and (111)Ge layers. Transmission electron microscopy studies showed the polycrystalline nature of CeO₂ film. X-ray photoelectron spectroscopy analysis showed multiple Ce3d and Ce4d oxidation states with a mixture of Ce³⁺ and Ce⁴⁺ components present inside the CeO₂ film. Angular resolved XPS investigations indicated that Ce³⁺ oxidation states preferred to be present near the surface of the oxide film and the PVD deposited CeO₂ films mostly consisted of Ce⁴⁺ oxidation states. Valence band offset values of 1.6, 1.5, and 1.6 eV were obtained from CeO₂/(100)Ge, CeO₂/(110)Ge, and CeO₂/(111)Ge, respectively, using XPS measurements from Ce3d core level peaks. Shallow Ce4d CL binding energy peaks were also used to verify the valence band offset values, and the results are in close agreement with those obtained from Ce3d peaks. The conduction band offset values between CeO₂/Ge are ~1.3 eV using the measured optical bandgap of CeO₂. The XPS analysis and band offset studies of CeO₂/Ge with different Ge orientations would offer important guidance for future design of Ge-based metal–oxide–semiconductor devices.

ACKNOWLEDGMENTS

This work was supported in part by National Science Foundation under Grant No. ECCS-1348653. The authors (S.P., D.M., and R.V.) acknowledge the financial support from Office of Basic Energy Science, Department of Energy, through Grant No. DE-FG02-06ER46290. Authors would also like to thank Jerry Hunter and Andrew Giordani, Virginia Tech, for assisting angular resolved XPS measurements.

¹N. Yang, W. K. Henson, and J. J. Wortman, *Proceedings of IEEE International Electron Devices Meeting (IEDM)* (IEEE, Baltimore, MD, 2009), p. 453.

- ²S. H. Lo, D. A. Buchanan, Y. Taur, and W. I. Wang, *IEEE Electron Device Lett.* **18**, 209 (1997).
- ³Y. Zhu and M. K. Hudait, "Low-power tunnel field effect transistors using mixed As and Sb based heterostructures," *Nanotechnol. Rev.* **2**, 637 (2013).
- ⁴M. K. Hudait, Y. Zhu, D. Maurya, and S. Priya, *Appl. Phys. Lett.* **102**, 093109 (2013).
- ⁵M. K. Hudait and Y. Zhu, *J. Appl. Phys.* **113**, 114303 (2013).
- ⁶M. K. Hudait, Y. Zhu, D. Maurya, S. Priya, P. K. Patra, A. W. K. Ma, A. Aphale, and I. Macwan, *J. Appl. Phys.* **113**, 134311 (2013).
- ⁷M. S. Rahman, E. K. Evangelou, I. I. Androulidakis, and A. Dimoulas, *Electrochem. Solid-State Lett.* **12**, H165 (2009).
- ⁸W.-C. Shih, C.-H. Chen, F.-C. Chiu, C.-M. Lai, and H.-L. Hwang, *ECS Trans.* **28**, 435 (2010).
- ⁹V. V. Afanas'ev, S. Shamuilia, A. Stesmans, A. Dimoulas, Y. Panayiotatos, A. Sotiropoulos, M. Houssa, and D. P. Brunco, *Appl. Phys. Lett.* **88**, 132111 (2006).
- ¹⁰Y. Nishikawa, D. Matsushita, N. Satou, M. Yoshiki, T. Schimizu, T. Yamaguchi, H. Satake, and N. Fukushima, *J. Electrochem. Soc.* **151**, F202 (2004).
- ¹¹M. K. Hudait, Y. Zhu, N. Jain, S. Vijayaraghavan, A. Saha, T. Merritt, and G. A. Khodaparast, *J. Vac. Sci. Technol., B* **30**, 051205 (2012).
- ¹²M. K. Hudait, Y. Zhu, N. Jain, and J. J. L. Hunter, *J. Vac. Sci. Technol., B* **31**, 011206 (2013).
- ¹³D. P. Brunco *et al.*, *J. Appl. Phys.* **102**, 024104 (2007).
- ¹⁴W.-H. Kim, W. J. Maeng, M.-K. Kim, J. Gatineau, and H. Kim, *J. Electrochem. Soc.* **158**, G217 (2011).
- ¹⁵J. Robertson and B. Falabretti, *J. Appl. Phys.* **100**, 014111 (2006).
- ¹⁶M. Baron, O. Bondarchuk, D. Stacchiola, S. Shaikhutdinov, and H. J. Freund, *J. Phys. Chem C* **113**, 6042 (2009).
- ¹⁷J. Rebellato, M. M. Natile, and A. Glisenti, *Appl. Catal., A* **339**, 108 (2008).
- ¹⁸A. Q. Wang, P. Panchaipetch, R. M. Wallace, and T. D. Golden, *J. Vac. Sci. Technol., B* **21**, 1169 (2003).
- ¹⁹P. Burroughs, A. Hamnett, A. F. Orchard, and G. Thornton, *J. Chem. Soc., Dalton Trans.* **1976**, 1686 (1976).
- ²⁰J. H. Choi, Y. Mao, and J. P. Chang, *Mater. Sci. Eng., R* **72**, 97 (2011).
- ²¹S. Dissanayake, K. Tomiyama, S. Sugahara, M. Takenaka, and S. Takagi, *Appl. Phys. Express* **3**, 041302 (2010).
- ²²M. Perego and G. Seguini, *J. Appl. Phys.* **110**, 053711 (2011).
- ²³M. Perego, A. Molle, and G. Seguini, *Appl. Phys. Lett.* **101**, 211606 (2012).
- ²⁴W. F. Zhang, T. Nishimura, K. Nagashio, K. Kita, and A. Toriumi, *Appl. Phys. Lett.* **102**, 102106 (2013).
- ²⁵C. Anandan and P. Bera, *Appl. Surf. Sci.* **283**, 297 (2013).
- ²⁶D. R. Mullins, S. H. Overbury, and D. R. Huntley, *Surf. Sci.* **409**, 307 (1998).
- ²⁷K.-D. Schierbaum, *Surf. Sci.* **399**, 29 (1998).
- ²⁸E. J. Preisler, O. J. Marsh, R. A. Beach, and T. C. McGill, *J. Vac. Sci. Technol., B* **19**, 1611 (2001).
- ²⁹T. Ueno and A. Odajima, *Jpn. J. Appl. Phys., Part 2* **21**, 230 (1982).
- ³⁰T. Ueno, *Jpn. J. Appl. Phys., Part 2* **22**, 1349 (1983).
- ³¹E. A. Kraut, R. W. Grant, J. R. Waldrop, and S. P. Kowalczyk, *Phys. Rev. Lett.* **44**, 1620 (1980).
- ³²Y. Zhu, N. Jain, D. K. Mohata, S. Datta, D. Lubyshev, J. M. Fastenau, A. K. Liu, and M. K. Hudait, *J. Appl. Phys.* **113**, 024319 (2013).
- ³³Y. Zhu, N. Jain, D. K. Mohata, S. Datta, D. Lubyshev, J. M. Fastenau, A. K. Liu, and M. K. Hudait, *Appl. Phys. Lett.* **101**, 112106 (2012).
- ³⁴Y. Zhu *et al.*, *J. Appl. Phys.* **112**, 094312 (2012).
- ³⁵J. Tauc, R. Grigorovici, and A. Vancu, *Phys. Status Solidi B* **15**, 627 (1966).
- ³⁶A. Dimoulas *et al.*, *Thin Solid Films* **515**, 6337 (2007).
- ³⁷J. W. Seo, P. C. McIntyre, S. Sun, D. I. Lee, P. Pianetta, and K. C. Saraswat, *Appl. Phys. Lett.* **87**, 221906 (2005).
- ³⁸S. J. Lee, C. Zhu, and D. L. Kwong, in *Advanced Gate Stacks for High-Mobility Semiconductors*, edited by A. Dimoulas, E. Gusev, P. C. McIntyre, and M. Heyns (Springer, Berlin, 2007).
- ³⁹T. Ami, Y. Ishida, N. Nagasawa, A. Machida, and M. Suzuki, *Appl. Phys. Lett.* **78**, 1361 (2001).
- ⁴⁰Y. T. Ho, K. S. Chang, K. C. Liu, L. Z. Hsieh, and M. H. Liang, *Crystr. Res. Technol.* **48**, 308 (2013).
- ⁴¹M. M. Hasan, A. S. M. A. Haseeb, R. Saidur, and H. H. Masjuki, *World Acad. Sci., Eng. Technol.* **16**, 221 (2008).

- ⁴²T. V. Semikina, *Semicond. Phys., Quantum Electron. Optoelectron.* **7**, 291 (2004).
- ⁴³L. Truffault *et al.*, *Mater. Res. Bull.* **45**, 527 (2010).
- ⁴⁴S. Maensiri, C. Masingboon, P. Laokul, W. Jareonboon, V. Promarak, P. L. Anderson, and S. Seraphin, *Cryst. Growth Des.* **7**, 950 (2007).
- ⁴⁵F. Le Normand, L. Hilaire, K. Kili, G. Krill, and G. Maire, *J. Phys. Chem.* **92**, 2561 (1988).
- ⁴⁶F. Zhang, P. Wang, J. Koberstein, S. Khalid, and S. W. Chan, *Surf. Sci.* **563**, 74 (2004).
- ⁴⁷T. Shripathi and M. V. R. Rao, *J. Electron Spectrosc. Relat. Phenom.* **87**, 121 (1997).